

---

# Scene Transformer: A unified multi-task model for behavior prediction and planning

---

Jiquan Ngiam <sup>\*,1</sup>, Benjamin Caine <sup>\*,1</sup>, Vijay Vasudevan <sup>\*,1</sup>,  
 Zhengdong Zhang <sup>1</sup>, Hao-Tien Lewis Chiang <sup>2</sup>, Jeffrey Ling <sup>2</sup>,  
 Rebecca Roelofs <sup>1</sup>, Alex Bewley <sup>1</sup>, Chenxi Liu <sup>2</sup>, Ashish Venugopal <sup>2</sup>,  
 David Weiss <sup>2</sup>, Ben Sapp <sup>2</sup>, Zhifeng Chen <sup>1</sup>, Jonathon Shlens <sup>1</sup>

<sup>1</sup> Google Brain, <sup>2</sup> Waymo  
 {jngiam, bencaine, vrv}@google.com

## Abstract

Predicting the future motion of multiple agents is necessary for planning in dynamic environments. This task is challenging for autonomous driving since agents (e.g., vehicles and pedestrians) and their associated behaviors may be diverse and influence each other. Most prior work has focused on first predicting independent futures for each agent based on all past motion, and then planning against these independent predictions. However, planning against fixed predictions can suffer from the inability to represent the future interaction possibilities between different agents, leading to sub-optimal planning. In this work, we formulate a model for predicting the behavior of all agents jointly in real-world driving environments in a unified manner. Inspired by recent language modeling approaches, we use a masking strategy as the query to our model, enabling one to invoke a single model to predict agent behavior in many ways, such as potentially conditioned on the goal or full future trajectory of the autonomous vehicle or the behavior of other agents in the environment. Our model architecture fuses heterogeneous world state in a unified Transformer architecture by employing attention across road elements, agent interactions and time steps. We evaluate our approach on autonomous driving datasets for behavior prediction, and achieve state-of-the-art performance. Our work demonstrates that formulating the problem of behavior prediction in a unified architecture with a masking strategy may allow us to have a single model that can perform multiple motion prediction and planning related tasks effectively.

## 1 Introduction

Motion planning in a dense real-world urban environment is a mission-critical problem for deploying autonomous driving technology. The autonomous driving task is traditionally considered too difficult for a single end-to-end learned system [53]. Thus, researchers have opted to split the task into sequential sub-tasks [62]: (i) perception, (ii) behavior prediction, and (3) planning. Perception is the task of detecting and tracking objects in the scene from sensor inputs such as LiDARs and cameras. Behavior prediction [24, 1, 6, 9, 12, 14, 16, 20, 26, 33, 35, 38, 39, 64] involves predicting the futures actions of other agents in the scene, while planning [3, 62, 46] involves creating a motion plan that navigates through dynamic environments.

Dividing the larger problem into sub-tasks achieves optimal performance when each sub-task is truly independent. However such a strategy breaks down when this assumption does not hold. For instance, the sub-tasks of behavior prediction and planning are not truly independent—the

---

\* Denotes equal contribution. Please see author contributions section for details.

autonomous vehicle’s actions may significantly impact the behaviors of other agents. Similarly, the behaviors of other agents may dramatically change what is a good plan. In this work, we introduce an approach that performs both behavior prediction and planning in a single framework, enabling the model to intrinsically capture these dependencies between the two tasks.

A prerequisite of such a multi-task system is that it needs to be able to jointly predict the futures of multiple agents (including the autonomous vehicle), while simultaneously taking into account their interactions. While the behavior prediction task has traditionally been formulated around per-agent independent predictions, recent datasets [19, 63] have introduced interaction prediction tasks that enable us to study joint future prediction. These interaction prediction tasks require that models predict the joint futures of multiple agents: models are expected to produce future predictions for all agents such that the agents futures are consistent<sup>1</sup> within each future.

A naive approach to producing joint futures is to consider the exponential number of combinations of *marginal* agent predictions. In this work, we instead present a single unified model that predicts a distribution over joint futures for all agents across time in a single inference pass. Importantly, this approach can capture the interactions between agents, and allows the model to be trained simultaneously to perform both behavior prediction and planning. Our model uses a global representation for all agents in an environment [33, 26, 12, 47] to allow scaling to large numbers of agents in dense environments. We employ a simple variant of self-attention [56] in which the attention mechanism is efficiently factorized across the agent-time axes. The resulting architecture simply alternates attention between dimensions representing time and agents across the scene, resulting in a computationally-efficient, uniform, and scalable architecture.

We find that the resulting model, termed *Scene Transformer*, achieves superior performance on both independent (marginal) and interactive (joint) prediction benchmarks. We further show how we can use a masking strategy, inspired by recent advances in language modeling [7, 17], to train a multi-task model that performs both behavior prediction and planning. The masking strategies allow us to adapt what data the model has access to at input time, such that the masks corresponds to different tasks.

We hope that this work provides a compelling example for how predicting joint, consistent futures of all agents in an environment opens new opportunities for critical tasks in autonomous vehicle technology. In summary, our key contributions in this work are:

- A unified multi-task training and inference framework in which a single model can accomplish the tasks of behavior prediction, conditional behavior prediction, and goal-directed planning.
- A novel, scene-centric approach to representing joint future distributions over multiple agents in a single feed-forward network.
- A Transformer-based architecture factored over agents, time, and road graph elements that exploits the inherent dependencies of the problem. The resulting architecture is generic and integrates the world state in a unified way.

## 2 Related Work

**Behavior Modeling Architectures.** Behavior prediction models have flourished in recent years, due to the rise in interest in self-driving applications and the release of related datasets and benchmarks [30, 15, 10, 19]. Models must take into account road graph elements and their relationships (e.g., lanes, stop lines, traffic light dynamic state), a history of agent motion, relationships between agents, and the road network.

One class of models draws heavily upon the computer vision literature, rendering inputs as a multi-channel rasterized top-down image [16, 14, 33, 26, 12, 47]. In this approach, relationships between scene elements are captured via convolutional deep architectures. However, the localized structure of the receptive field makes capturing spatially-distant interactions challenging. As a popular alternative is to use an entity-centric approach. In these works, agent state history is typically encoded via sequence modeling techniques like RNNs [39, 31, 33, 1, 45] or temporal convolutions [35]. Road elements are approximated with basic primitives (e.g. piecewise-linear segments) which encode pose information and semantic type. Modeling relationships between entities is often presented as an

---

<sup>1</sup>Marginal agent predictions may conflict with each other (have overlaps), while consistent joint predictions should have predictions where agents respect each other’s behaviors (avoid overlaps) within the same future.

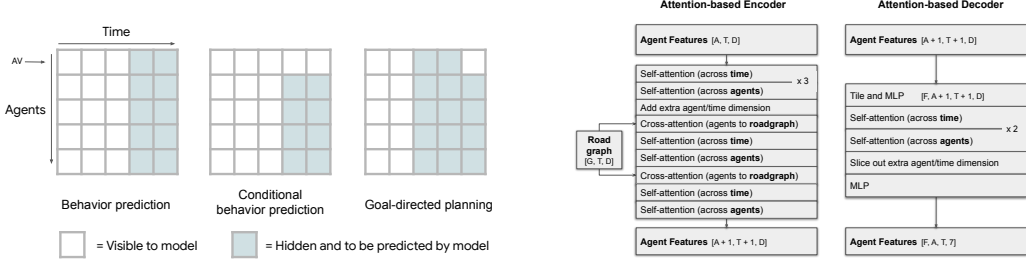


Figure 1: **Single model architecture for multiple navigation tasks.** Left: Different masking strategies define distinct tasks. The left column represents current time and the top row represents the agent indicating the autonomous vehicle (AV). A single model can be trained for data associated with behavior prediction, conditional behavior prediction, and goal-directed planning, by matching the masking strategy to each prediction task. Right: Attention-based encoder-decoder architecture for joint scene modeling. Architecture employs factored attention along the time and agent axes to exploit the dependencies in the data, and cross-attention to inject side information.

information aggregation process, and models employ pooling [64, 20, 33, 1, 24], soft-attention [39, 64, 47] as well as graph neural networks [12, 35, 31].

Like our proposed method, several recent models use Transformers [56], composed of multi-headed attention layers. Transformers are a popular state-of-the-art choice for sequence modeling in natural language processing [7, 17], and have recently shown promise in core computer vision tasks such as detection [5, 11, 49], tracking [27] and classification [44, 55, 18, 4, 5]. For behavior modeling, recent work has employed variations of self-attention and Transformers for modeling different axes: temporal trajectory encoding and decoding [60, 22, 61], encoding relationships between agents [34, 61, 60, 39], and encoding relationships with road elements. When applying self-attention over multiple axes, past work used independent self-attention for each axis [60], or flattened two axes together into one joint self-attention layer [61] – by comparison, our method proposes axis-factored attention to model relationships between time steps, agents, and road graph elements in a unified way.

**Scene-centric versus agent-centric representations.** Another key design choice is the frame of reference in which the representation is encoded. Some models do a majority of modeling in a global, scene-level coordinate frame, such as work that employs a rasterized top-down image [16, 14, 33, 26, 12, 47]. This can lead to a more efficient model due to a single shared representation of world state in a common coordinate frame, but comes with the potential sacrifice of pose-invariance. On the other hand, models that reason in the agent-coordinate frame [39, 64, 31] are intrinsically pose-invariant, but scale linearly with the number of agents, or quadratically with the number of pairwise interactions between agents. Many works employ a mix of a top-down raster representation for road representation fused with a per-agent representations [45, 52, 33]. Similar to our own work, LaneGCN [35] is agent-centric yet representations are in a global frame – to the best of our knowledge, this is the only other work to do so. This enables efficient reasoning while capturing arbitrarily distant interactions and high-fidelity state representations without rasterization.

**Representing multi-agent futures.** The most common way to represent agent futures is via a weighted set of trajectories per agent [1, 6, 9, 12, 12, 14, 16, 20, 26, 33, 33, 38, 39, 47, 64]. This representation is encouraged by benchmarks which primarily focus on per-agent distance error metrics [10, 15, 63]. We argue in this work that modeling *joint* futures in a multi-agent environment is an important concept that has been minimally explored in prior work. Some prior work consider a factorized pairwise joint distribution, where a subset of agent futures are conditioned on other agents – informally, modeling  $P(X)$  and  $P(Y|X)$  for agents  $X$  and  $Y$  [31, 54, 47]. To generalize joint prediction to arbitrary multi-agent settings, other prior work [52, 45, 13, 50, 59] iteratively roll out samples per-agent, where each agent is conditioned on previously sampled trajectory steps. In contrast, our model directly decodes a set of  $k$  distinct joint futures with associated likelihoods.

### 3 Methods

The Scene Transformer model has three stages: (i) Embed the agents and the road graph into a high dimensional space, (ii) Employ an attention-based network to encode the interactions between agents and the road graph, (iii) Decode multiple futures using an attention-based network. The model takes as input a feature for every agent at every time step, and also predicts an output for every agent at every time step. We have an associated hidden mask, where every agent time step has an associated indicator of 1 (hidden) or 0 (visible), indicating whether the input feature is hidden (i.e. removed) from the model. This approach mirrors the approach of masked-language models such as BERT [17]. The approach is flexible, enabling us to simultaneously train a single model for *behavior prediction (BP)* [16, 14, 33, 26, 12, 47, 12, 35, 31], *conditional behavior prediction (CBP)* [31, 54, 47] and *goal-directed planning (GDP)* [62, 36] simply by changing what data is shown to the model.

**Multi-task representation.** The key representation in the model is a 3-dimensional tensor of  $A$  agents with  $D$  feature dimensions across  $T$  time steps. At every layer within the architecture, we aim to maintain a representation of shape  $[A, T, D]$ , or when decoding,  $[F, A, T, D]$  across  $F$  potential futures. Each task (BP, CBP, GDP) can be formulated as a query with a specific masking strategy by setting the indicator mask to 0, thus exposing that data to the model. (Figure 1, left panel). The goal of the model is to impute the features for each shaded region corresponding to subsets of time and agents in the scenario that are masked. Note that we additionally employ data augmentation to boost performance as detailed in the Appendix.

#### 3.1 High dimensional embeddings for agents and road graphs.

Our model has three different distinct sets of features it must encode before passing them off to the encoding transformer. We summarize the MLP-based architecture below, and provide further details about the architecture in the Appendix. First, we generate a feature for every agent time step if that time step is visible. Second, we generate a set of features for the static road graph, road elements static in space and time, learning one feature vector *per polyline* (with signs being polylines of length 1) using a PointNet [43]. Lastly, we generate a set of features for the dynamic road graph, which are road elements static in space but dynamic in time (e.g. traffic lights), also one feature vector per object. All three categories have *xyz* position information, which we preprocess to center and rotate around the agent of interest<sup>2</sup>.

#### 3.2 Encoding transformer

We focus on a simple encoder-decoder attention-based architecture which maintains a representation of  $[A, T, D]$  throughout (Figure 1, right). We summarize the architecture briefly, but reserve details for the Appendix and Table 3. The majority of layers are a form of the Transformer layer [56] (Table 4). Attention layers are parameterized as matrices representing the query  $Q$ , key  $K$ , and value  $V$ , whose output  $y = \text{softmax} \frac{(Q K^T) V}{\sqrt{dim_k}}$ . Each matrix is computed as a learned linear transformation of the underlying representation  $x$ , e.g.  $Q = W_q x$ . Each attention layer is followed by a feed-forward layer of the same hidden dimension, and a skip connection addition of the result with the input to the whole Transformer layer. All layers of the encoder and decoder employ a  $D$  feature dimension. The final layer after the decoder is a 2-layer MLP that predicts 7 outputs. The first 6 outputs correspond to the 3-dimensional position of an agent at a given time step in absolute coordinates (e.g. meters), and the corresponding uncertainty parameterized by a Laplace distribution [40]. The remaining dimension predicts the heading.

**Efficient factorized self-attention.** The bulk of the computation is performed with a Transformer [56] (Table 4). One naive approach to use the Transformer would be to perform attention directly on the entire set of agent and time step features (i.e., attention across  $AT$  dimensions). However, this approach is computationally expensive, and also suffers from an identity symmetry challenge: two agents of the same type hidden at the same future location will have their input representations be exactly alike. Thus, we design a *factorized* attention based on the time and agents axes (for related ideas, see [57, 51, 25]). Applying attention only across time allows the model to learn smooth

<sup>2</sup>For WOMD, we center the scene with respect to the autonomous vehicle (AV). For Argoverse, we center the scene with respect to the agent that needs to be predicted. Both are centered around what would be the last visible time step in a behavior prediction setup for all tasks.

trajectories independent of the identity of the agent. Likewise, applying attention only across agents allows the model to learn multi-agent interactions independent of the specific time step. Finally, in order to capture both time and agent dependencies, the model simply alternates attention across agents and time in subsequent layers (Figure 1, right panel).

**Cross-attention.** In order to exploit side information, which in our case is a road graph, we use cross-attention to enable the agent features to be updated by attending to the road graph. Concretely, we calculate the queries from the agents, but the keys and values come from the embeddings of the road graph. The road graph embeddings are also *not* updated during these attention layers. This requires that the model learn interactions between the road structure and agents that are independent of the specific time step. We highlight that the road graph representation is shared across all agents in the scene, whereas prior approaches have often used an agent-centric road graph representation.

### 3.3 Predicting probabilities for each futures.

Our model also needs to predict a probability score for each trajectory. In order to do so, we need a feature representation that summarizes the scene and each agent. To accomplish this, we generate an artificial agent and time step and add this to the agent features representation (Figure 1, left panel). After the first set of factorized self-attention layers, we compute the mean of the agent features tensor across the agent and time dimension separately, and add these as an additional artificial agent and time. This artificial agent and time step propagates through the network. At the final layer, we slice out the artificial agent and time step to obtain summary features for each agent (the additional time per agent), and for the scene (the ‘corner’ feature that is both additional time and agent). This feature is then processed by a 2-layer MLP producing a single logit value that we use with a softmax classifier.

### 3.4 Joint and marginal loss formulation.

The output of our model is a tensor of shape  $[F, A, T, 7]$  representing the location and heading of each agent at the given time step. Because the model uses a scene-centric representation for the locations through positional embeddings, the model is able to predict all agents simultaneously in a single feed-forward pass. This design also makes it possible to have a straight-forward switch between joint future predictions and marginal future predictions.

To perform joint future prediction, we treat each future (in the first dimension) to be coherent futures across all agents. Thus, we aggregate the displacement loss across all agents<sup>3</sup> and time steps to build a loss tensor of shape  $[F]$ . We only back-propagate the loss through the individual future that most closely matches the ground-truth in terms of displacement loss [24, 59]. For marginal future predictions, each agent is treated independently. After computing the displacement loss of shape  $[F, A]$ , we do *not* aggregate across agents. Instead, we select the future with minimum loss for each agent separately, and back-propagate the error correspondingly. This allows the agents to select among different futures. One notable benefit of our approach is that we are able to produce predictions for all agent simultaneously.

**Evaluation metrics for behavior prediction.** We evaluate the quality of  $k$  weighted trajectory hypotheses using the standard evaluation metrics: minADE, minFDE, miss rate, and mAP. Each evaluation metric attempts to measure how close the top  $k$  trajectories are to ground truth observation. A simple and common distance-based metric is to measure the  $L_2$  norm between a given trajectory and the ground truth [1, 42]. minADE reports the  $L_2$  norm of the trajectory with the minimal distance. minFDE likewise reports the  $L_2$  norm of the trajectory with the smallest distance only evaluated at the final location of the trajectory. We additionally report the miss rate (MR) and mean average precision (mAP) to capture how well a model predicts all of the future trajectories of agents probabilistically [59, 15, 19]. For joint future evaluation settings, we measure the scene-level equivalents (minSADE, minSFDE, and SMR) that evaluate the prediction of the best single consistent future [13].

---

<sup>3</sup>Each dataset provides a subset of agents it asks to be predicted, which are the only ones we include in our loss. For Argoverse this is one agent, and for the WOMD it is 2-8 per scene.

Method	minADE ↓	minFDE ↓	MR ↓
Jean [39]	0.97	1.42	0.13
WIMP [31]	0.90	1.42	0.17
TNT [64]	0.94	1.54	0.13
LaneGCN [35]	0.87	1.36	0.16
TPCN [58]	0.85	1.35	0.16
mmTransformer [37]	0.84	1.34	0.15
HOME [21]	0.94	1.45	<b>0.10</b>
Scene Transformer (Ours)	<b>0.80</b>	<b>1.23</b>	0.13

Table 1: **Predictive performance on Argoverse behavior prediction.** Results reported on *test* split for vehicles [15]. Reported are the minADE, minFDE for  $k = 6$  predictions [1, 42], and the Miss Rate (MR) [15] within 2 meters of the target. All results are reported for  $t = 3$  seconds. Since the task specifies only one agent to predict per scene, marginal and joint are equivalent with our method.

## 4 Results

We train the Scene Transformer on behavior prediction tasks from the Waymo Open Motion Dataset (WOMD) [19] and the Argoverse dataset [15]. The WOMD dataset consists of 104,000 run segments (each 20 seconds in duration) over 1,750 km of unique roadways containing 7.64 million unique agent tracks. The Argoverse dataset consists of 324,000 run segments (each 5 seconds in duration) over 290 km of unique roadways containing 11.7 million unique agent tracks. Each model is trained on a Cloud TPU [29] (See Appendix for all training details). We demonstrate that the resulting model achieves best published performance across these datasets.

For the Argoverse dataset, we train and evaluate the model solely on the behavior prediction task. Thus, we only employ the behavior prediction mask (Figure 1, left) for training the model. For the WOMD we train the model with all masks jointly, selecting a mask strategy for each batch uniformly at random. We evaluate the WOMD on behavior prediction, conditional behavior prediction and goal-directed planning. For all models, we evaluate the quality of  $k$  weighted trajectory hypotheses using a suite of standard evaluation metrics (See Methods).

### 4.1 Behavior prediction

**Argoverse.** The Argoverse task requires that we predict a single agent. We use a masking strategy that provides the model with all the agents as input, but with their futures masked out. During training, the model is only required to predict the future of the single agent of interest. Our best Argoverse model uses  $D = 512$  feature dimensions and label smoothing for trajectory classification. Our model achieves state-of-the-art results compared to published<sup>4</sup> prior work in terms of minADE/minFDE (Table 1).

**Waymo Open Motion Dataset (WOMD).** Next we evaluate the performance of our model with  $D = 256$  on the recently released Waymo Open Motion Dataset [19]. WOMD provides two separate evaluation tasks with unique metrics and associated validation and test data sets. The first task is the *Motion Prediction* challenge, which is a standard motion forecasting task where up to 8 of the scene’s agents are chosen to have their top 6 trajectory predictions evaluated independently. The second is the *Interaction Prediction* challenge, which tasks the model with predicting the trajectories of two interacting agents *jointly*. The metrics for the *Interaction Prediction* task are *joint* variations of the common minADE, minFDE, and Miss Rate metrics, and measure the quality of the joint prediction of both agents within up to 6 predicted futures.

To fully compare the marginal and joint formulations of our model, we evaluate the product of these models and datasets. That is, we evaluate the marginal model on the *Motion Prediction* challenge, and then evaluate it on the *Interaction Prediction* challenge by converting our marginal predictions to joint ones mirroring the methodology in [19]<sup>5</sup>. We then evaluate our joint model on the *Motion Prediction* challenge to see how it would fare as a marginal model, despite being trained to solve

<sup>4</sup>We chose to exclude comparing to public leaderboard entries that have not been published since their details are not available, but note that our results are competitive on the leaderboard as of the submission date.

<sup>5</sup>We take the top 6 pairs of trajectories from the combination of both agent’s trajectories for 36 total pairs.

<b>Motion Prediction</b>	minADE $\downarrow$			minFDE $\downarrow$			veh	ped	cyc	MR $\downarrow$	mAP $\uparrow$	
	veh	ped	cyc	veh	ped	cyc						
<i>valid</i>												
LSTM baseline [19]	1.34	0.63	1.26	2.85	1.35	2.68	0.25	0.13	0.29	0.23	0.23 <b>0.20</b>	
ours (marginal)	<b>1.17</b>	<b>0.59</b>	<b>1.15</b>	<b>2.51</b>	<b>1.26</b>	<b>2.44</b>	<b>0.20</b>	<b>0.12</b>	<b>0.24</b>	<b>0.26</b>	<b>0.27</b> <b>0.20</b>	
ours (joint, bp-only)	1.53	0.90	1.63	3.48	2.09	3.77	0.28	0.30	0.37	0.20	0.16	0.13
ours (joint, multi-task)	1.56	0.89	1.60	3.56	2.06	3.68	0.29	0.29	0.37	0.19	0.15	0.15
<i>test</i>												
LSTM baseline [19]	1.34	0.64	1.29	2.83	1.35	2.68	0.24	0.13	0.29	0.24	0.22	0.19
ours (marginal)	<b>1.17</b>	<b>0.60</b>	<b>1.17</b>	<b>2.48</b>	<b>1.25</b>	<b>2.43</b>	<b>0.19</b>	<b>0.12</b>	<b>0.22</b>	<b>0.27</b>	<b>0.23</b> <b>0.20</b>	
ours (joint, bp-only)	1.52	0.91	1.61	3.43	2.09	3.68	0.28	0.30	0.37	0.19	0.16	0.19
ours (joint, multi-task)	1.55	0.91	1.64	3.50	2.08	3.75	0.28	0.29	0.38	0.19	0.16	0.19

<b>Interaction Prediction</b>	minSADE $\downarrow$			minSFDE $\downarrow$			veh	ped	cyc	SMR $\downarrow$	mAP $\uparrow$
	veh	ped	cyc	veh	ped	cyc					
<i>valid</i>											
LSTM baseline [19]	2.42	2.73	3.16	6.07	4.20	6.46	0.66	1.00	0.83	0.07	<b>0.06</b> 0.02
ours (marginal)	2.04	1.62	2.28	4.94	3.81	5.67	0.54	0.63	0.72	<b>0.11</b>	0.05 0.03
ours (joint, bp-only)	<b>1.72</b>	<b>1.38</b>	1.96	<b>3.98</b>	<b>3.11</b>	4.75	<b>0.49</b>	<b>0.60</b>	0.73	<b>0.11</b>	0.05 0.03
ours (joint, multi-task)	<b>1.72</b>	1.39	<b>1.94</b>	3.99	3.15	<b>4.69</b>	<b>0.49</b>	0.62	<b>0.71</b>	<b>0.11</b>	<b>0.06</b> <b>0.04</b>
<i>test</i>											
LSTM baseline [19]	2.46	2.47	2.96	6.22	4.30	6.26	0.67	0.89	0.89	0.06	0.03 0.03
ours (marginal)	2.08	1.62	2.24	5.04	3.87	5.41	0.55	0.64	0.73	0.08	<b>0.05</b> 0.03
ours (joint, bp-only)	1.76	<b>1.38</b>	<b>1.95</b>	4.08	<b>3.19</b>	<b>4.65</b>	<b>0.50</b>	<b>0.62</b>	<b>0.70</b>	0.10	<b>0.05</b> <b>0.04</b>
ours (joint, multi-task)	<b>1.74</b>	1.41	<b>1.95</b>	<b>4.06</b>	3.26	4.68	<b>0.50</b>	0.64	0.71	<b>0.13</b>	0.04 0.03

Table 2: **Predictive performance on Waymo Open Motion Dataset behavior prediction** [19]. Top: Marginal predictive performance based on the *standard* splits of the validation and test datasets. Bottom: Joint predictive performance based on the *interactive* splits of the validation and test datasets. Reported are the min(S)ADE, min(S)FDE for  $k = 6$  predictions [1, 42], and the Miss Rate (MR) [15] within 2 meters of the target. Results for the *Motion Prediction* section use traditional marginal metrics, while results for the *Interaction Prediction* use joint, scene-level variants of these metrics (see [19]). All results are reported at  $t = 8$  seconds. See Appendix for  $t = 3$  and  $t = 5$  seconds.

the harder joint problem, and then we evaluate it as a true joint model using joint metrics on the *Interaction Prediction* challenge.

We find that the marginal model achieves state-of-the-art performance over the provided baseline (Table 4, top) on the *Motion Prediction* challenge, demonstrating the strength of our general architecture. We next show that the same architecture, instead trained with the joint loss formulation, performs worse on marginal metrics on the same *Motion Prediction* challenge. The story flips when we look at the *Interaction Prediction* challenge (Table 4, bottom), which evaluates the model’s joint predictions with joint scene-level metrics. Our joint model easily outperforms both the baseline [19] and our own marginal model’s predictions converted to joint predictions on metrics such as minSADE [13]. This shows that beyond the strength of our overall architecture and approach, that explicitly training a model as a joint model significantly improves joint performance on joint metrics, at the cost of that models performance on marginal metrics. A notable observation is that even though the *Interaction Prediction* task only requires predicting the joint trajectories of two agents, our method is fully general and predicts joint consistent futures of all agents.

**Multi-task prediction.** The larger goal of this work is to develop a method amenable to solving multiple prediction tasks, including behavior prediction, conditional behavior prediction and goal-directed planning. We next ask if Scene Transformer can be trained as a multi-task model using the same architecture, but with a mix of masking strategies that correspond to each task. During training, we supply masks corresponding to the three tasks with a probability 1/3 each.

We find that the multi-task model trained with a joint loss achieves behavior prediction metrics comparable to the joint prediction model (Table 4) trained on BP only, despite being trained with additional masks for conditional behavior prediction and goal-directed planning. This indicates that a jointly-trained multi-task model is a viable strategy for solving many behavior prediction problems.

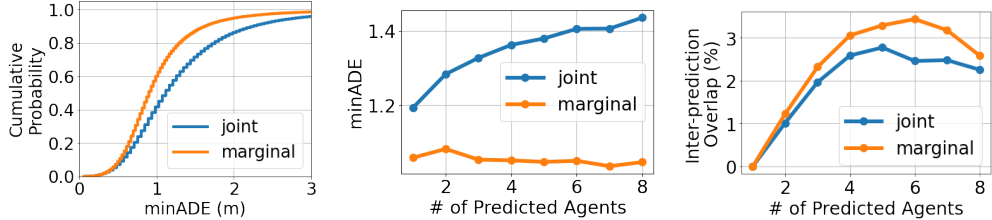


Figure 2: **Quantitative comparison of the marginal and joint prediction models.** Left: Cumulative distribution of the minADE for the marginal and joint models evaluated on the motion prediction task. The mean minADE for the marginal model is lower than the joint model (marginal =  $1.05m$  vs joint =  $1.35m$ ). Center: The minADE broken down as a function of number of predicted agents. When there are more agents, producing internally consistent predictions is more challenging, and hence the joint model performs slightly worse. Right: Overlap rate between pairs of agent predictions. The joint model produces internally consistent predictions with lower inter-prediction overlap rates.

#### 4.2 Understanding the trade-offs between the joint and marginal models

While the joint BP-only model performs better on the interactive prediction task than the marginal model, it performs worse on the motion prediction task. This is because the joint model is trained to produce predictions that are internally consistent between agents, while the marginal model does not. In this section, we examine this quality difference and the internal consistency of the predictions from both models.

In the WOMD dataset, each example has a different number of agents to be predicted. By slicing the *marginal* minADE results based on the number of agents to be predicted (Figure 2, center), we find that the joint model performs worse as there are more predicted agents, while the marginal model performs the same. This is expected: when there are more agents, the joint model has a more difficult task since it needs to produce internally consistent predictions. We note that this result is encouraging as it shows that the joint model may not need to predict an exponential number of trajectories to perform competitively with the marginal model.<sup>6</sup>

However, when more agents are to be predicted, the possibility of interactions are higher and we would expect that the joint model is able to capture these interactions through internally consistent predictions. We measure the models’ internal consistency by selecting the best trajectory and measuring the *inter-prediction overlap rate* (details in Appendix). We find that the joint model has a consistently lower inter-prediction overlap rate, showing that it is able to capture the interactions between agents. The ability to model interactions enables the model to be suitable for CBP and GDP tasks, which we discuss in following sections.

#### 4.3 Conditional behavior prediction with a multi-task model

Given that the joint prediction model better captures interactions, we next investigate the additional benefits in training a multi-task model trained on BP, CBP, and GDP. We train a single multi-task model, where each task is presented during training 1/3 of the time, and run it at inference with different masks to evaluate its ability to perform different tasks.

The CBP task provides the model with the full trajectory of a single specified agent, and requires the model to produce future trajectories for the other agents. We focus on the interactive split of WOMD in order to provide a meaningful test bed for CBP. To fairly compare to BP, for each scene we average the two agents’ minADE when conditioned on the ground truth of the other. We compare the same multi-task model’s performance in both BP and CBP inference modes. The CBP minADE is 0.09 lower than the BP counterpart (1.25 vs 1.34), demonstrating that Scene Transformer is able to utilize useful information from the future (when available) to improve behavior prediction.

<sup>6</sup>One might expect a joint model to need an exponential number of trajectories to match the combinatorial possibilities of a marginal model. However, when many agents are interacting, the number of realistic scenarios can be more constrained by the interactions.

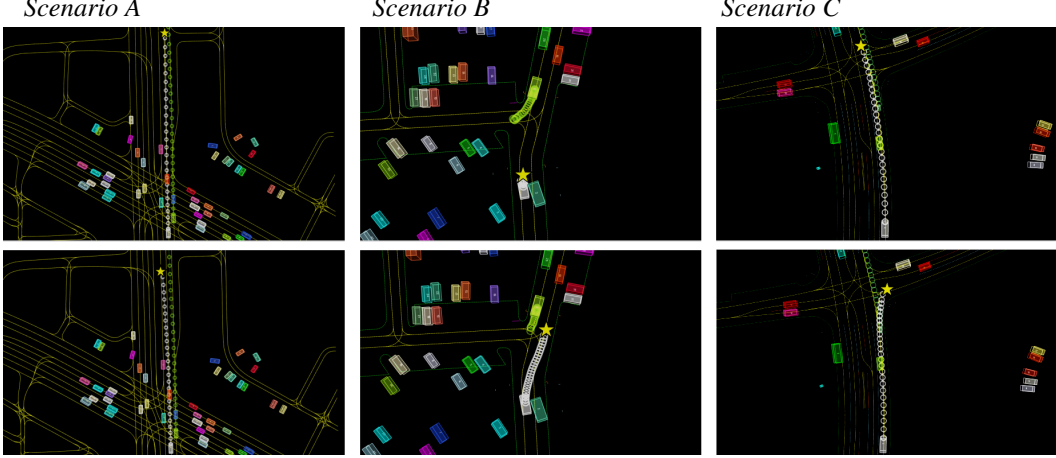


Figure 3: **Goal-directed planning navigates AV to selected goal positions.** Rectangles indicate vehicles on the road. Lines indicate the road graph (RG) colored by the type of lane marker. Circles indicate predicted trajectory for each agent. Star indicates selected goal for AV. Each column represents a scenario in which the AV is directed to perform one of two actions taking into account the dynamics of other agents. (A) AV instructed to either change lanes or remain in the same lane. (B) AV instructed to stop to allow oncoming vehicle to turn left, or adjust to the side in a narrow passage so that the oncoming vehicle has enough space to pass. (C) AV instructed to either proceed straight or turn right at the intersection.

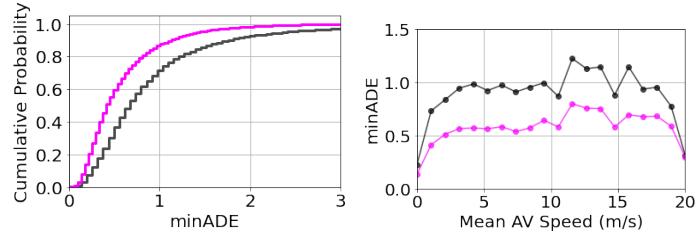


Figure 4: **Analysis of the multi-task model for goal-directed planning.** Left: Cumulative probability of the AV minADE in planning (blue) and BP (black) masking strategies. Right: AV minADE for planning (blue) and BP (black) as a function of AV speed (averaged over the ground truth trajectory).

#### 4.4 Goal-directed planning with a multi-task model

We next examine how the *same* multi-task model in the previous section performs on goal-directed planning (GDP). Specifically, we want to aid a full planning system that evaluates potential AV goal destinations by providing consistent, joint futures of all agents. We supply the model at inference time with a GDP mask where the final position of the AV is specified along with the state history of AV and all agents (Figure 1), and ask the model to fill in the AV trajectory. This task is less well-defined in the literature, but as a proof of principle we showcase several visualizations of the multi-task model in goal-directed scenarios. Qualitatively, we demonstrate that our model produces reasonable trajectories to arrive at the goal positions, even when they differ from the ground truth, across a diverse repertoire of behaviors (Figure 3). Critically, we observe that AV goal conditioning impacts the predicted behavior of *other agents* in a consistent, realistic manner.

Quantitatively, we verify that our model can effectively use the privileged information of the final ground truth endpoint by re-purposing the behavior prediction metrics for measuring the performance of the AV prediction. We compare the performance of the multi-task model under two different masking strategies *at inference time*: (1) A masking strategy for behavior prediction and (2) A masking strategy for goal-directed planning. We find that the minADE for the AV is decreased for the interactive split of the WOMD (Figure 4) when the privileged information is made available to the multi-task model. When we break down the minADE across AV speeds, we find that the

gains of employing a goal-directed planning mask are most pronounced at lower speeds, peaking at roughly  $2\times$  reduction in minADE. This latter property is particularly advantageous as many complex interactive maneuvers occur in crowded environments at low speeds.

## 5 Discussion

We propose a unified architecture for autonomous driving that is able to model the complex interactions of agents in the environment. Our approach is amenable to multi-task learning and a single model can perform behavior prediction, conditional behavior prediction, and goal-directed planning. In the field of autonomous driving, elaborations of this problem formulation may result in learning models for planning systems that quantitatively improve upon existing systems [8, 41, 65, 62]. Likewise, such modeling efforts may be used to directly go after issues of identifying interacting agents in an environment, and potentially provide an important task for identifying causal relationships [2, 48].

## Acknowledgements

We thank Dragomir Anguelov, Scott Ettinger, Yuning Chai, Andre Cornman, Rami Al-Rfou, Mark Palatucci, Balakrishnan Varadarajan, Barret Zoph, and Shuyang Cheng for their comments and suggestions. Additionally, we thank the larger Google Brain, Google Perception, and Waymo Applied Research teams for their support.

## Author Contributions

JN conceived of the modeling approach. JN, VV and BC co-led the project and developed models, infrastructure, experiments, evaluations, and analysis. ZZ developed several architecture innovations that led to notable improvements, and ran many experiments to tune, optimize and improve the model performance. HC developed several modeling and novel data augmentation innovations that led to notable improvements, and ran many experiments to improve model performance. AB ran many experiments to improve the performance of the marginal predictions of the model, and analyzed the relative performance of the marginal and joint prediction model. RR led much of the analysis of the model performance, and investigated the robustness of the model architectures. CL ran experiments to improve the overall performance of the model, and led much of the experiments and analysis on conditional behavior prediction. JL, DW and AV led the experiments focused on goal-directed planning. BS offered much discussion and ideas surrounding behavior prediction, and helped write the paper. ZC helped develop the infrastructure and provided guidance and mentorship. JS helped write the paper, coordinate the project, and provide guidance and mentorship.

## References

- [1] A. Alahi, K. Goel, V. Ramanathan, A. Robicquet, L. Fei-Fei, and S. Savarese. Social LSTM: Human trajectory prediction in crowded spaces. In *Proceedings of the IEEE conference on computer vision and pattern recognition*, pages 961–971, 2016.
- [2] M. Arjovsky, L. Bottou, I. Gulrajani, and D. Lopez-Paz. Invariant risk minimization. *arXiv preprint arXiv:1907.02893*, 2019.
- [3] M. Bansal, A. Krizhevsky, and A. Ogale. Chauffeurnet: Learning to drive by imitating the best and synthesizing the worst. In *Proceedings of Robotics: Science and Systems*, FreiburgimBreisgau, Germany, June 2019.
- [4] I. Bello. LambdaNetworks: Modeling long-range interactions without attention. In *International Conference on Learning Representations (ICLR)*, 2013.
- [5] I. Bello, B. Zoph, A. Vaswani, J. Shlens, and Q. V. Le. Attention augmented convolutional networks. In *Proceedings of the IEEE/CVF International Conference on Computer Vision*, pages 3286–3295, 2019.
- [6] Y. Biktairov, M. Stebelev, I. Rudenko, O. Shliazhko, and B. Yangel. Prank: motion prediction based on ranking. In *Advances in neural information processing systems*, 2020.
- [7] T. B. Brown, B. Mann, N. Ryder, M. Subbiah, J. Kaplan, P. Dhariwal, A. Neelakantan, P. Shyam, G. Sastry, A. Askell, et al. Language models are few-shot learners. In *Advances in Neural Information Processing Systems*, 2020.
- [8] M. Buehler, K. Iagnemma, and S. Singh. *The DARPA urban challenge: autonomous vehicles in city traffic*, volume 56. Springer, 2009.
- [9] T. Buhet, E. Wirbel, and X. Perrotton. Plop: Probabilistic polynomial objects trajectory planning for autonomous driving. In *Conference on Robot Learning*, 2020.
- [10] H. Caesar, V. Bankiti, A. H. Lang, S. Vora, V. E. Liou, Q. Xu, A. Krishnan, Y. Pan, G. Baldan, and O. Beijbom. nuscenes: A multimodal dataset for autonomous driving. In *Proceedings of the IEEE/CVF Conference on Computer Vision and Pattern Recognition*, pages 11621–11631, 2020.
- [11] N. Carion, F. Massa, G. Synnaeve, N. Usunier, A. Kirillov, and S. Zagoruyko. End-to-end object detection with transformers. In *European Conference on Computer Vision*, pages 213–229. Springer, 2020.

- [12] S. Casas, C. Gulino, R. Liao, and R. Urtasun. Spagnn: Spatially-aware graph neural networks for relational behavior forecasting from sensor data. In *2020 IEEE International Conference on Robotics and Automation, ICRA 2020, Paris, France, May 31 - August 31, 2020*, pages 9491–9497. IEEE, 2020.
- [13] S. Casas, C. Gulino, S. Suo, K. Luo, R. Liao, and R. Urtasun. Implicit latent variable model for scene-consistent motion forecasting. In *Proceedings of the European Conference on Computer Vision (ECCV)*. Springer, 2020.
- [14] Y. Chai, B. Sapp, M. Bansal, and D. Anguelov. Multipath: Multiple probabilistic anchor trajectory hypotheses for behavior prediction. In *Conference on Robot Learning*, 2019.
- [15] M.-F. Chang, J. Lambert, P. Sangkloy, J. Singh, S. Bak, A. Hartnett, D. Wang, P. Carr, S. Lucey, D. Ramanan, et al. Argoverse: 3d tracking and forecasting with rich maps. In *Proceedings of the IEEE/CVF Conference on Computer Vision and Pattern Recognition*, pages 8748–8757, 2019.
- [16] H. Cui, V. Radosavljevic, F.-C. Chou, T.-H. Lin, T. Nguyen, T.-K. Huang, J. Schneider, and N. Djuric. Multimodal trajectory predictions for autonomous driving using deep convolutional networks. In *2019 International Conference on Robotics and Automation (ICRA)*, pages 2090–2096. IEEE, 2019.
- [17] J. Devlin, M.-W. Chang, K. Lee, and K. Toutanova. Bert: Pre-training of deep bidirectional transformers for language understanding. In *Conference of the North American Chapter of the Association for Computational Linguistics*, 2019.
- [18] A. Dosovitskiy, L. Beyer, A. Kolesnikov, D. Weissenborn, X. Zhai, T. Unterthiner, M. Dehghani, M. Minderer, G. Heigold, S. Gelly, et al. An image is worth 16x16 words: Transformers for image recognition at scale. In *International Conference on Learning Representations (ICLR)*, 2021.
- [19] S. Ettinger, S. Cheng, B. Caine, C. Liu, H. Zhao, S. Pradhan, Y. Chai, B. Sapp, C. Qi, Y. Zhou, et al. Large scale interactive motion forecasting for autonomous driving: The waymo open motion dataset. *arXiv preprint arXiv:2104.10133*, 2021.
- [20] J. Gao, C. Sun, H. Zhao, Y. Shen, D. Anguelov, C. Li, and C. Schmid. VectorNet: Encoding hd maps and agent dynamics from vectorized representation. In *Proceedings of the IEEE/CVF Conference on Computer Vision and Pattern Recognition*, 2020.
- [21] T. Gilles, S. Sabatini, D. Tsishkou, B. Stanciulescu, and F. Moutarde. HOME: heatmap output for future motion estimation. *CoRR*, abs/2105.10968, 2021.
- [22] F. Giuliani, I. Hasan, M. Cristani, and F. Galasso. Transformer networks for trajectory forecasting. In *International Conference on Pattern Recognition*, 2020.
- [23] X. Glorot and Y. Bengio. Understanding the difficulty of training deep feedforward neural networks. In *Proceedings of the thirteenth international conference on artificial intelligence and statistics*, pages 249–256. JMLR Workshop and Conference Proceedings, 2010.
- [24] A. Gupta, J. Johnson, L. Fei-Fei, S. Savarese, and A. Alahi. Social GAN: Socially acceptable trajectories with generative adversarial networks. In *CVPR*, 2018.
- [25] J. Ho, N. Kalchbrenner, D. Weissenborn, and T. Salimans. Axial attention in multidimensional transformers. *arXiv preprint arXiv:1912.12180*, 2019.
- [26] J. Hong, B. Sapp, and J. Philbin. Rules of the road: Predicting driving behavior with a convolutional model of semantic interactions. In *CVPR*, 2019.
- [27] W.-C. Hung, H. Kretzschmar, T.-Y. Lin, Y. Chai, R. Yu, M.-H. Yang, and D. Anguelov. Soda: Multi-object tracking with soft data association. *arXiv preprint arXiv:2008.07725*, 2020.
- [28] S. Ioffe and C. Szegedy. Batch normalization: Accelerating deep network training by reducing internal covariate shift. In *International conference on machine learning*, pages 448–456. PMLR, 2015.
- [29] N. P. Jouppi, C. Young, N. Patil, D. Patterson, G. Agrawal, R. Bajwa, S. Bates, S. Bhatia, N. Boden, A. Borchers, et al. In-datacenter performance analysis of a tensor processing unit. In *Proceedings of the 44th annual international symposium on computer architecture*, pages 1–12, 2017.

- [30] R. Kesten, M. Usman, J. Houston, T. Pandya, K. Nadhamuni, A. Ferreira, M. Yuan, B. Low, A. Jain, P. Ondruska, S. Omari, S. Shah, A. Kulkarni, A. Kazakova, C. Tao, L. Platinsky, W. Jiang, and V. Shet. Lyft level 5 perception dataset 2020. <https://level5.lyft.com/dataset/>, 2019.
- [31] S. Khandelwal, W. Qi, J. Singh, A. Hartnett, and D. Ramanan. What-if motion prediction for autonomous driving. *arXiv preprint arXiv:2008.10587*, 2020.
- [32] D. P. Kingma and J. Ba. Adam: A method for stochastic optimization. In *International Conference on Learning Representations (ICLR)*, 2015.
- [33] N. Lee, W. Choi, P. Vernaza, C. B. Choy, P. H. Torr, and M. Chandraker. Desire: Distant future prediction in dynamic scenes with interacting agents. In *Proceedings of the IEEE Conference on Computer Vision and Pattern Recognition*, pages 336–345, 2017.
- [34] L. L. Li, B. Yang, M. Liang, W. Zeng, M. Ren, S. Segal, and R. Urtasun. End-to-end contextual perception and prediction with interaction transformer. In *IEEE/RSJ International Conference on Intelligent Robots and Systems (IROS)*, 2020.
- [35] M. Liang, B. Yang, R. Hu, Y. Chen, R. Liao, S. Feng, and R. Urtasun. Learning lane graph representations for motion forecasting. In *European Conference on Computer Vision (ECCV)*, 2020.
- [36] J. Liu, W. Zeng, R. Urtasun, and E. Yumer. Deep structured reactive planning. *arXiv preprint arXiv:2101.06832*, 2021.
- [37] Y. Liu, J. Zhang, L. Fang, Q. Jiang, and B. Zhou. Multimodal motion prediction with stacked transformers, 2021.
- [38] F. Marchetti, F. Becattini, L. Seidenari, and A. D. Bimbo. Mantra: Memory augmented networks for multiple trajectory prediction. In *Proceedings of the IEEE/CVF Conference on Computer Vision and Pattern Recognition*, pages 7143–7152, 2020.
- [39] J. Mercat, T. Gilles, N. Zoghby, G. Sandou, D. Beauvois, and G. Gil. Multi-head attention for joint multi-modal vehicle motion forecasting. In *IEEE International Conference on Robotics and Automation*, 2020.
- [40] G. P. Meyer and N. Thakurdesai. Learning an uncertainty-aware object detector for autonomous driving. In *IEEE/RSJ International Conference on Intelligent Robots and Systems (IROS)*, pages 10521–10527, 2020.
- [41] M. Montemerlo, J. Becker, S. Bhat, H. Dahlkamp, D. Dolgov, S. Ettinger, D. Haehnel, T. Hilden, G. Hoffmann, B. Huhnke, et al. Junior: The stanford entry in the urban challenge. *Journal of field Robotics*, 25(9):569–597, 2008.
- [42] S. Pellegrini, A. Ess, K. Schindler, and L. Van Gool. You’ll never walk alone: Modeling social behavior for multi-target tracking. In *2009 IEEE 12th International Conference on Computer Vision*, pages 261–268. IEEE, 2009.
- [43] C. R. Qi, H. Su, K. Mo, and L. J. Guibas. Pointnet: Deep learning on point sets for 3d classification and segmentation. In *Proceedings of the IEEE conference on computer vision and pattern recognition*, pages 652–660, 2017.
- [44] P. Ramachandran, N. Parmar, A. Vaswani, I. Bello, A. Levskaya, and J. Shlens. Stand-alone self-attention in vision models. In *Advances in Neural Information Processing Systems*, volume 32, 2019.
- [45] N. Rhinehart, R. McAllister, K. Kitani, and S. Levine. Precog: Prediction conditioned on goals in visual multi-agent settings. In *Proceedings of the IEEE/CVF International Conference on Computer Vision*, pages 2821–2830, 2019.
- [46] A. Sadat, S. Casas, M. Ren, X. Wu, P. Dhawan, and R. Urtasun. Perceive, predict, and plan: Safe motion planning through interpretable semantic representations. In *ECCV*, pages 414–430. Springer, 2020.
- [47] T. Salzmann, B. Ivanovic, P. Chakravarty, and M. Pavone. Trajectron++: Dynamically-feasible trajectory forecasting with heterogeneous data. *arXiv preprint arXiv:2001.03093*, 2020.
- [48] B. Schölkopf, F. Locatello, S. Bauer, N. R. Ke, N. Kalchbrenner, A. Goyal, and Y. Bengio. Toward causal representation learning. *Proceedings of the IEEE*, 2021.

- [49] A. Srinivas, T.-Y. Lin, N. Parmar, J. Shlens, P. Abbeel, and A. Vaswani. Bottleneck transformers for visual recognition. In *CVPR*, 2021.
- [50] S. Suo, S. Regalado, S. Casas, and R. Urtasun. Trafficsim: Learning to simulate realistic multi-agent behaviors. In *Conference on Computer Vision and Pattern Recognition (CVPR)*, 2021.
- [51] C. Szegedy, V. Vanhoucke, S. Ioffe, J. Shlens, and Z. Wojna. Rethinking the inception architecture for computer vision. In *Proceedings of the IEEE conference on computer vision and pattern recognition*, pages 2818–2826, 2016.
- [52] C. Tang and R. R. Salakhutdinov. Multiple futures prediction. In *NeurIPS*, 2019.
- [53] S. Thrun, M. Montemerlo, H. Dahlkamp, D. Stavens, A. Aron, J. Diebel, P. Fong, J. Gale, M. Halpenny, G. Hoffmann, et al. Stanley: The robot that won the darpa grand challenge. *Journal of field Robotics*, 23(9):661–692, 2006.
- [54] E. Tolstaya, R. Mahjourian, C. Downey, B. Vadarajan, B. Sapp, and D. Anguelov. Identifying driver interactions via conditional behavior prediction. *2021 IEEE International Conference on Robotics and Automation (ICRA)*, 2021.
- [55] A. Vaswani, P. Ramachandran, A. Srinivas, N. Parmar, B. Hechtman, and J. Shlens. Scaling local self-attention for parameter efficient visual backbones. In *CVPR*, 2021.
- [56] A. Vaswani, N. Shazeer, N. Parmar, J. Uszkoreit, L. Jones, A. N. Gomez, L. Kaiser, and I. Polosukhin. Attention is all you need. *arXiv preprint arXiv:1706.03762*, 2017.
- [57] H. Wang, Y. Zhu, B. Green, H. Adam, A. Yuille, and L.-C. Chen. Axial-deeplab: Stand-alone axial-attention for panoptic segmentation. In *European Conference on Computer Vision*, pages 108–126. Springer, 2020.
- [58] M. Ye, T. Cao, and Q. Chen. Tpcn: Temporal point cloud networks for motion forecasting. *arXiv preprint arXiv:2103.03067*, 2021.
- [59] R. A. Yeh, A. G. Schwing, J. Huang, and K. Murphy. Diverse generation for multi-agent sports games. In *Proceedings of the IEEE/CVF Conference on Computer Vision and Pattern Recognition*, pages 4610–4619, 2019.
- [60] C. Yu, X. Ma, J. Ren, H. Zhao, and S. Yi. Spatio-temporal graph transformer networks for pedestrian trajectory prediction. In *European Conference on Computer Vision*, pages 507–523. Springer, 2020.
- [61] Y. Yuan, X. Weng, Y. Ou, and K. Kitani. Agentformer: Agent-aware transformers for socio-temporal multi-agent forecasting. *arXiv preprint arXiv:2103.14023*, 2021.
- [62] W. Zeng, W. Luo, S. Suo, A. Sadat, B. Yang, S. Casas, and R. Urtasun. End-to-end interpretable neural motion planner. In *Proceedings of the IEEE/CVF Conference on Computer Vision and Pattern Recognition*, pages 8660–8669, 2019.
- [63] W. Zhan, L. Sun, D. Wang, H. Shi, A. Clausse, M. Naumann, J. Kümmerle, H. Königshof, C. Stiller, A. de La Fortelle, and M. Tomizuka. INTERACTION Dataset: An INTERnational, Adversarial and Cooperative moTION Dataset in Interactive Driving Scenarios with Semantic Maps. *arXiv:1910.03088 [cs, eess]*, 2019.
- [64] H. Zhao, J. Gao, T. Lan, C. Sun, B. Sapp, B. Varadarajan, Y. Shen, Y. Shen, Y. Chai, C. Schmid, et al. Tnt: Target-driven trajectory prediction. *arXiv preprint arXiv:2008.08294*, 2020.
- [65] J. Ziegler, P. Bender, T. Dang, and C. Stiller. Trajectory planning for bertha—a local, continuous method. In *2014 IEEE intelligent vehicles symposium proceedings*, pages 450–457. IEEE, 2014.

## Supplementary Materials

### A Architecture and Training Details

**Overview.** Table 3 provides additional details about the Scene Transformer architecture and training. The bulk of the computation and parameters reside in the Transformer layers. Table 4 lists all of the operations and learned parameters in our implementation of a Transformer. MLPs are employed to embed the original data (e.g., layers  $A$ ,  $B$ ,  $C$ ), build  $F$  futures from the encoding (layer  $T$ ), and predict the final position, headings and uncertainties of all agents (layers  $Z_1$  and  $Z_2$ ). The resulting attention-based architecture using  $D = 256$  feature dimensions contains 15,296,136 parameters. Nearly all settings used for both WOMD and Argoverse are identical, except that for Argoverse we use  $D = 512$  and label smoothing to get our best marginal results. The resulting model is trained on a TPU custom hardware accelerator [29] and converges in about 3 days of training.

**Decoding multiple futures.** In order to allow the decoder to output  $F$  distinct futures, we perform the following operations. The decoder receives as input a tensor of shape  $[A, T, D]$  corresponding to  $A$  agents across  $T$  time steps and  $D$  feature dimensions. The following series of simple operations restructures the representation to predict  $F$  futures. First, the representation is copied across  $F$  dimensions to generate  $[F, A, T, D]$ . We append on a one-hot encoding to the final dimension where a 1 indicates which of the  $F$  futures is the ground truth trajectory resulting in a tensor of shape  $[F, A, T, D + F]$ . The one-hot encoding allows the network to learn an embedding for each of the  $F$  futures. For computational simplicity, the resulting representation is propagated through a small MLP to produce a return a tensor of the shape  $[F, A, T, \bar{D}]$ .

**Padding and Hidden Masks.** Padding and hidden masks are important to get right in the implementation of such a model. In particular, we need to ensure that the masks do not convey additional future information to the model (e.g., if the model knows which timesteps an agent is visible or occluded based on the padding in the data, it may take advantage of this and not be able to generalize). We use the concept of padding to indicate the positions where the *input* is absent or provided. This is distinct from the hidden mask of shape  $[A, T]$  that is used for *task specification*. The hidden mask is used to query the model to inform it on which locations to predict, while the padding tells us which locations have inputs and ground-truth to compute a loss over. All padded positions are set to be hidden during preprocessing, regardless of the masking scheme, so the model tries to predict their values. All layers in our implementation are padding aware, including normalization layers (like batch normalization used in our encoding MLPs) and attention operations. Our attention operations set the attention weights to 0 for padded elements. If after providing our task specific hidden mask, no non-padded (valid) time steps exist for an agent, the whole agent is set to be padded. This prevents agent slots with no valid data from being used in the model.

**Predicting uncertainties.** For each predicted variate such as position or heading, we additionally predict a corresponding uncertainty. In early experiments we found that predicting a paired uncertainty improves the predictive performance of the original variate and provides a useful signal for interpreting the fidelity of the predicted value. We employ a loss function that predicts a parameterization of the uncertainty corresponding to a Laplace distribution [40].

**Loss in lateral and longitudinal coordinates.** We use a Laplace distribution parameterization for the loss, with a diagonal covariance such that each axis is independent. To enable the model to learn meaningful uncertainties, we rotate the scene per box prediction such that each prediction’s associated ground-truth is axis aligned. This formulation results in uncertainty estimates that correspond to the agent’s lateral and longitudinal coordinates.

**Marginal predictions from a joint model.** The model has the added feature of being easily adapted for making marginal predictions for each agent. To produce per-trajectory scores for each agents predictions, we attach an artificial extra time step to the end of the  $[A, T, D]$  agent feature matrix to give us a matrix of shape  $[A, T + 1, D]$ . This artificial feature can learn a per-agent representation we can use to predict which of the  $k$  trajectories most closely matches the ground truth for that agent.

**Data augmentation.** We use two methods for data augmentation to aid generalization and combat overfitting on both datasets. First, we use agent dropout, where we artificially remove non-predicted agents with some probability. We found a probability of 0.1 worked well for both datasets. We also found it beneficial to randomly rotate the entire scene between  $[-\frac{\pi}{2}, \frac{\pi}{2}]$  after centering to the agent of

interest. On Argoverse, this agent of interest is the agent the task designates to be predicted, where as on the WOMD we always center around the autonomous vehicle (AV), even though for some tasks it is not one of the predicted agents. Lastly, each Argoverse scene contains many agents that the model is not required to predict; we employ these contextual agents as additional target training data if the contextual agents moved by at least 6m.

**Argoverse classification label smoothing:** Our best model on Argoverse uses  $D = 512$  feature dimensions, but naively scaling the model this way leads to severe overfitting on the classification subtask. During training of our best model we employ label smoothing ( $0.1 + 1/6$  for negatives and  $0.9 + 1/6$  for positive target).

**Measuring agent inter-prediction overlap.** We measure *predicted* agent overlap on the best set of trajectory produced by the model. For the joint model, this corresponds to the joint prediction that has the higher probability score. For the marginal model, we take the top scoring trajectory for each agent to obtain the best set. For every predicted agent in the trajectory, we determine if it has an overlap with any *other predicted* agent by comparing the rotated upright 3D bounding boxes using our predicted xyz and heading. The inter-prediction overlap rate is the number of predicted agents that are involved in some overlap, divided by the total number of predicted agents. We count two agents as overlapping if the intersection over the union (IoU) exceeds 0.01.

**Embedding of agents and road graph.** To generate input features, we use sinusoidal positional embeddings [56] to embed the time (for agents and dynamic roadgraph) and *xyz*-coordinates separately into a  $D$  dimensional features per dimension. We encode the type of each object using a one-hot encoding (e.g. object type, lane type, etc), and concatenate any other features provided in the data set such as yaw, width, length, height, and velocity. Dynamic road graphs have a second one-hot encoding indicating state, like the traffic light state. Lastly, for agents and the dynamic road graph, we add a binary indicator on whether the agent is hidden at that time step. If the agent or dynamic road graph element is hidden, all input features (e.g. position, type, velocity, state, etc) are set to 0 before encoding except the time embedding, which are linearly spaced values at the dataset's update rate starting at 0, and the hidden indicator.

For agents and the dynamic road graph, we use a 2 layer MLP with a hidden and output dimension of  $D$  to produce a final feature per agent or object and per time step. For the static road graph, we must reduce a point cloud of up to 20,000 road graph points, each belonging to a smaller set of polylines, to a single vector per polyline. Because some lanes can be extremely long, we break up any polyline longer than 20 points into a new set of smaller polylines. Then, we apply a small PointNet [43] architecture with a 2 layer MLP with a hidden and output dimension of  $D$  to each point, and use max pooling per polyline to get a final feature per element.

Meta-Arch	Name	Input	Operation	Queries	Keys/Values	Across	Atten Matrix	Output Size	# Param
<b>Encoder</b>									
$\mathcal{A}$	Agents	MLP + BN	–	–	–	–	$[A, T, D]$	334080	
$\mathcal{B}$	Dyna RG	MLP + BN	–	–	–	–	$[G_D, T, D]$	337408	
$\mathcal{C}$	Static RG	MLP + BN	–	–	–	–	$[G_S, T, D]$	270592	
$\mathcal{D}$	$\mathcal{A}, \mathcal{B}, \mathcal{C}$	Transformer	Agents	Agents	Time	$[A, T, T]$	$[A, T, D]$	789824	
$\mathcal{E}$	$\mathcal{D}$	Transformer	Agents	Agents	Agents	$[T, A, A]$	$[A, T, D]$	789824	
$\mathcal{F}$	$\mathcal{E}$	Transformer	Agents	Agents	Time	$[A, T, T]$	$[A, T, D]$	789824	
$\mathcal{G}$	$\mathcal{F}$	Transformer	Agents	Agents	Agents	$[T, A, A]$	$[A, T, D]$	789824	
$\mathcal{H}$	$\mathcal{G}$	Transformer	Agents	Agents	Time	$[A, T, T]$	$[A, T, D]$	789824	
$\mathcal{I}$	$\mathcal{H}$	Transformer	Agents	Agents	Agents	$[T, A, A]$	$[A, T, D]$	789824	
$\mathcal{J}$	$\mathcal{I}$	Transformer	Agents	Static RG	Time	$[T, A, G_S]$	$[A, T, D]$	789824	
$\mathcal{K}$	$\mathcal{J}$	Transformer	Agents	Dyna RG	Time	$[T, A, G_D]$	$[A, T, D]$	789824	
$\mathcal{L}$	$\mathcal{K}$	Transformer	Agents	Agents	Time	$[A, T, T]$	$[A, T, D]$	789824	
$\mathcal{M}$	$\mathcal{L}$	Transformer	Agents	Agents	Agents	$[T, A, A]$	$[A, T, D]$	789824	
$\mathcal{N}$	$\mathcal{M}$	Transformer	Agents	Static RG	Time	$[T, A, G_S]$	$[A, T, D]$	789824	
$\mathcal{O}$	$\mathcal{N}$	Transformer	Agents	Dyna RG	Time	$[T, A, G_D]$	$[A, T, D]$	789824	
$\mathcal{P}$	$\mathcal{O}$	Transformer	Agents	Agents	Time	$[A, T, T]$	$[A, T, D]$	789824	
$\mathcal{Q}$	$\mathcal{P}$	Transformer	Agents	Agents	Agents	$[T, A, A]$	$[A, T, D]$	789824	
<b>Decoder</b>									
$\mathcal{R}$	$\mathcal{Q}$	Tile	–	–	–	–	$[F, A, T, D]$	0	
$\mathcal{S}$	$\mathcal{R}$	Concat	–	–	–	–	$[F, A, T, D+F]$	0	
$\mathcal{T}$	$\mathcal{S}$	MLP	–	–	–	–	$[F, A, T, D]$	68096	
$\mathcal{U}$	$\mathcal{T}$	Transformer	Agents	Agents	Time	$[A, T, T]$	$[F, A, T, D]$	789824	
$\mathcal{V}$	$\mathcal{U}$	Transformer	Agents	Agents	Agents	$[T, A, A]$	$[F, A, T, D]$	789824	
$\mathcal{W}$	$\mathcal{V}$	Transformer	Agents	Agents	Time	$[A, T, T]$	$[F, A, T, D]$	789824	
$\mathcal{X}$	$\mathcal{W}$	Transformer	Agents	Agents	Agents	$[T, A, A]$	$[F, A, T, D]$	789824	
$\mathcal{Y}$	$\mathcal{X}$	Layer Norm	–	–	–	–	$[F, A, T, D]$	512	
$\mathcal{Z}_1$	$\mathcal{Y}$	MLP + BN	–	–	–	–	$[F, A, T, 6]$	66817	
$\mathcal{Z}_2$	$\mathcal{Y}$	MLP	–	–	–	–	$[F, A, T, 7]$	1799	
Optimizer	Adam [32] ( $\alpha = 1e-4$ , $\beta_1 = 0.9$ , $\beta_2 = 0.999$ )								
Learning Rate Schedule	Total epochs: 150; Linear ramp-up: 0.1 epochs								
Batch size	64								
Gradient Clipping (norm)	5								
Weight initialization	Xavier-Glorot [23]								
Weight decay	None								
Position Embeddings	Min Timescale: 4; Max Timescale: 256								
Temporal Embeddings	Min Timescale: 6; Max Timescale: 80								
Future classification weight	0.1								
Position classification weight	1.0								
Laplace Target Scale	1								

**Table 3: Scene Transformer architecture and training details.** The network receives as input of  $A$  agents across  $T$  time steps and  $K$  features.  $K$  is the total number of input features (e.g. 3-D position, velocity, object type, bounding box size). A subset of these inputs are masked.  $G_S$  and  $G_D$  is the maximum number of road graph (RG) elements and  $D$  is the total number of features. MLP and BN denote multilayer perception and batch normalization [28], respectively. The output of the network is  $\mathcal{Z}_1$  and  $\mathcal{Z}_2$ .  $\mathcal{Z}_1$  corresponds to predicting the logits for classifying which one of the  $F$  futures is most likely.  $\mathcal{Z}_2$  corresponds to the predicted  $xyz$ -coordinates with their associated uncertainties, and a single value for heading. In our model  $D = 256$ ,  $K = 7$  and  $F = 6$  for a total of 15,296,136 parameters for both datasets. For the Waymo Open Motion Dataset  $G_s = 1400$ ,  $G_d = 16$ ,  $T = 91$ ,  $A = 128$ , and for Argoverse  $G_s = 256$ ,  $G_d = 0$ ,  $T = 50$ , and  $A = 64$ . All layers employ ReLU nonlinearities.

Name	Input	Operation	Parameter Sizes	Output Size	# Param
$X$	$X_o$	Layer Norm	$[D], [D]$	$[A, T, D]$	512
$K$	$X$	Affine Projection	$[D, H, \frac{D}{H}], [H, \frac{D}{H}]$	$[A, T, H, \frac{D}{H}]$	65792
$V$	$X$	Affine Projection	$[D, H, \frac{D}{H}], [H, \frac{D}{H}]$	$[A, T, H, \frac{D}{H}]$	65792
$Q_o$	$X$	Affine Projection	$[D, H, \frac{D}{H}], [H, \frac{D}{H}]$	$[A, T, H, \frac{D}{H}]$	65792
$Q$	$Q_o$	Rescale	$[\frac{D}{H}]$	$[A, T, H, \frac{D}{H}]$	64
$Y_1$	$Q, K, V$	$\text{softmax}(Q K^T) V$	—	$[A, T, H, \frac{D}{H}]$	0
$Y_2$	$Y_1$	Affine Projection	$[H, \frac{D}{H}, D], [D]$	$[A, T, D]$	65792
$S$	$F_1, X_o$	Sum	—	$[A, T, D]$	0
$F_1$	$Y_2$	MLP	$[D, kD], [kD]$	$[A, T, kD]$	263168
$F_2$	$S$	MLP	$[kD, D], [D]$	$[A, T, D]$	262400
$Z$	$F_2$	Layer Norm	$[D], [D]$	$[A, T, D]$	512
<b>Total</b>					789824

Table 4: **Transformer architecture.** The network receives as input  $X_o$  and outputs  $Z$ . All MLP’s employ a ReLU nonlinearity.  $D$  is the number of feature dimensions;  $H$  is the number of attention heads. In our model  $D=256$ ,  $H=4$  and  $k=4$ .

## B Additional Behavior Prediction Results

Motion Prediction	minADE↓			minFDE↓			veh	ped	cyc	mAP↑
	veh	ped	cyc	veh	ped	cyc				
<i>valid</i>										
baseline [19]	0.39	0.19	0.41	0.65	0.36	0.73	0.14	0.07	0.25	0.33
ours (marginal)	<b>0.33</b>	<b>0.20</b>	<b>0.39</b>	<b>0.57</b>	<b>0.33</b>	<b>0.67</b>	<b>0.11</b>	<b>0.07</b>	<b>0.21</b>	<b>0.38</b>
ours (joint)	0.42	0.28	0.50	0.78	0.51	0.94	0.19	0.21	0.32	0.34
ours (multi-task joint)	0.43	0.51	0.51	0.80	0.52	0.93	0.20	0.21	0.32	0.33
<i>test</i>										
baseline [19]	0.39	0.20	0.41	0.65	0.36	0.74	0.14	0.07	0.25	0.34
ours (marginal)	<b>0.32</b>	<b>0.20</b>	<b>0.38</b>	<b>0.56</b>	<b>0.33</b>	<b>0.67</b>	<b>0.11</b>	<b>0.07</b>	<b>0.21</b>	<b>0.38</b>
ours (joint)	0.42	0.28	0.49	0.78	0.53	0.92	0.19	0.21	0.32	0.33
ours (multi-task joint)	0.44	0.29	0.50	0.80	0.53	0.93	0.20	0.22	0.32	0.32
Interaction Prediction	minSADE↓			minSFDE↓			veh	ped	cyc	mAP↑
	veh	ped	cyc	veh	ped	cyc				
<i>valid</i>										
baseline [19]	0.58	0.43	0.60	1.13	0.86	1.20	0.45	0.47	0.61	0.15
ours (marginal)	0.45	0.37	0.52	0.91	0.75	1.04	0.35	0.42	0.52	0.20
ours (joint)	0.41	<b>0.34</b>	<b>0.47</b>	0.81	<b>0.65</b>	0.92	<b>0.29</b>	<b>0.38</b>	<b>0.49</b>	0.26
ours (multi-task joint)	<b>0.40</b>	<b>0.34</b>	<b>0.47</b>	<b>0.80</b>	<b>0.65</b>	<b>0.91</b>	<b>0.28</b>	<b>0.38</b>	<b>0.49</b>	<b>0.27</b>
<i>test</i>										
baseline [19]	0.58	0.42	0.61	1.14	0.85	1.21	0.45	0.47	0.61	0.16
ours (marginal)	0.45	0.36	0.53	0.93	0.74	1.06	0.36	0.40	0.55	0.18
ours (joint)	<b>0.41</b>	<b>0.33</b>	<b>0.48</b>	0.82	<b>0.64</b>	<b>0.94</b>	<b>0.29</b>	<b>0.36</b>	<b>0.50</b>	0.18
ours (multi-task joint)	<b>0.41</b>	0.34	<b>0.48</b>	<b>0.81</b>	0.65	<b>0.94</b>	0.29	0.37	0.51	<b>0.26</b>

Table 5: **Predictive performance on Waymo Open Motion Dataset behavior prediction for  $t = 3$  seconds.** Please see Table 4 for details.

<b>Motion Prediction</b>	minADE $\downarrow$			minFDE $\downarrow$			veh	MR $\downarrow$	cyc	veh	mAP $\uparrow$
	veh	ped	cyc	veh	ped	cyc					
<i>valid</i>											
baseline [19]	0.74	0.37	0.75	1.36	0.73	1.43	0.17	0.10	0.25	0.29	<b>0.27</b> <b>0.26</b>
ours (marginal)	<b>0.65</b>	<b>0.35</b>	<b>0.69</b>	<b>1.23</b>	<b>0.67</b>	<b>1.30</b>	<b>0.15</b>	<b>0.10</b>	<b>0.22</b>	<b>0.33</b>	0.26 0.25
ours (joint)	0.83	0.51	0.93	1.68	1.08	1.91	0.23	0.26	0.33	0.26	0.19 0.18
ours (multi-task joint)	0.84	0.52	0.92	1.72	1.08	1.87	0.24	0.26	0.33	0.26	0.18 0.18
<i>test</i>											
baseline [19]	0.74	0.37	0.76	1.35	0.73	1.43	0.17	0.10	0.25	0.29	<b>0.26</b> <b>0.23</b>
ours (marginal)	<b>0.63</b>	<b>0.35</b>	<b>0.68</b>	<b>1.20</b>	<b>0.67</b>	<b>1.31</b>	<b>0.11</b>	<b>0.10</b>	<b>0.22</b>	<b>0.33</b>	<b>0.26</b> <b>0.23</b>
ours (joint)	0.83	0.52	0.91	1.68	1.10	1.88	0.23	0.26	0.33	0.26	0.19 0.22
ours (multi-task joint)	0.85	0.53	0.93	1.72	1.10	1.91	0.24	0.27	0.34	0.26	0.19 0.21
 <b>Interaction Prediction</b>											
<b>Interaction Prediction</b>	minSADE $\downarrow$			minSFDE $\downarrow$			veh	SMR $\downarrow$	cyc	veh	mAP $\uparrow$
	veh	ped	cyc	veh	ped	cyc					
<i>valid</i>											
baseline [19]	1.19	0.90	1.25	2.64	1.98	2.82	0.55	0.57	0.70	0.13	0.09 0.04
ours (marginal)	0.96	0.78	1.08	2.15	1.75	2.46	0.44	0.51	0.60	0.13	0.09 0.06
ours (joint)	0.84	0.68	0.95	1.81	1.45	2.09	<b>0.38</b>	<b>0.48</b>	<b>0.59</b>	0.18	0.08 <b>0.07</b>
ours (multi-task joint)	<b>0.83</b>	<b>0.68</b>	<b>0.95</b>	1.79	1.45	<b>2.08</b>	<b>0.38</b>	0.48	<b>0.59</b>	<b>0.19</b>	<b>0.10</b> 0.06
<i>test</i>											
baseline [19]	1.21	0.89	1.26	2.70	1.96	2.80	0.56	0.59	0.69	0.13	0.07 0.03
ours (marginal)	0.96	0.77	1.07	2.19	1.74	2.45	0.46	0.51	0.62	0.13	0.09 0.06
ours (joint)	0.85	<b>0.67</b>	<b>0.96</b>	1.85	<b>1.44</b>	2.10	<b>0.39</b>	0.50	<b>0.58</b>	0.17	<b>0.10</b> 0.07
ours (multi-task joint)	<b>0.84</b>	0.68	0.97	<b>1.82</b>	1.46	<b>2.09</b>	<b>0.39</b>	<b>0.49</b>	0.59	<b>0.20</b>	0.09 <b>0.08</b>

Table 6: **Predictive performance on Waymo Open Motion Dataset behavior prediction for  $t = 5$  seconds.** Please see Table 4 for details.

### C Slicing results

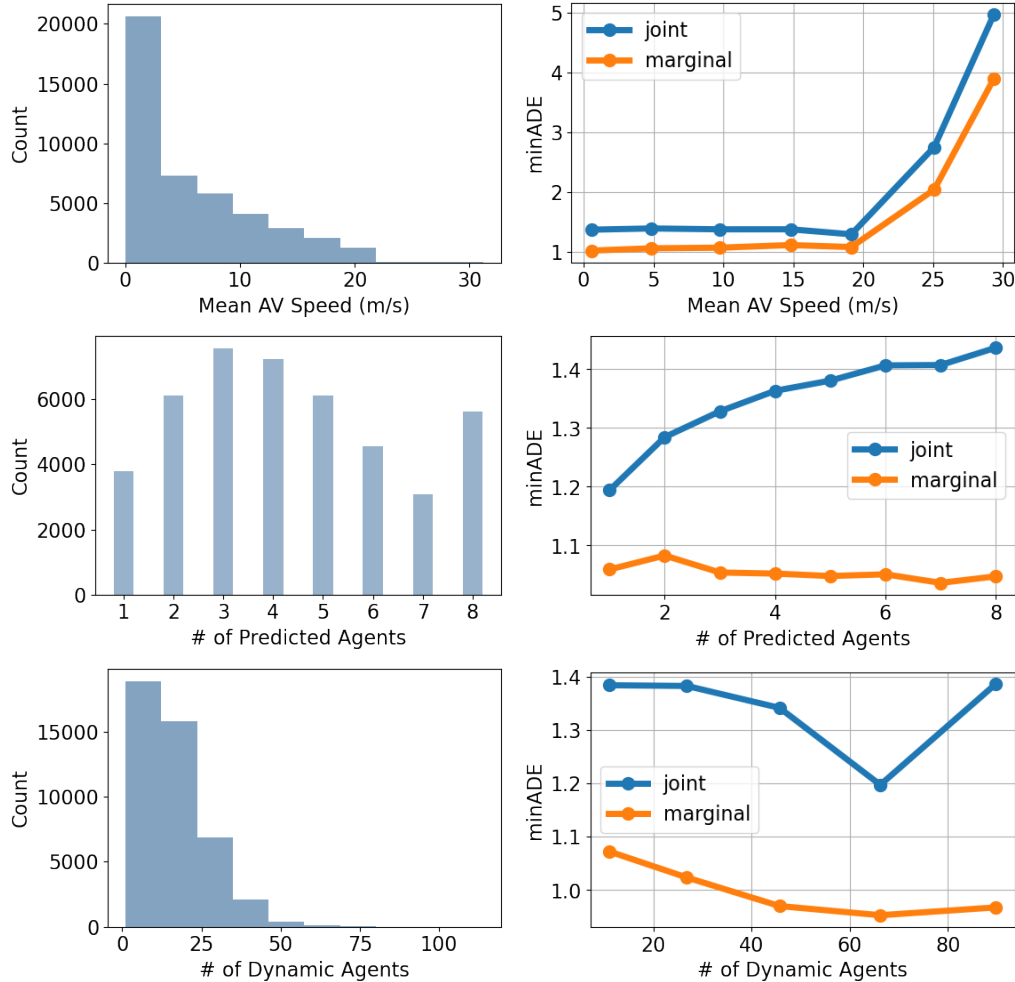


Figure 5: We show marginal minADE on a per scene basis broken down by different scene level statistics. Interestingly, we show that both the marginal and joint models become out of distribution above 20 m/s, where there is minimal training data.